

1    **Validation and field application of a low-cost device to measure CO<sub>2</sub>**  
2    **and ET fluxes**

3    Reena Macagga<sup>1</sup>, Michael Asante<sup>2, 3</sup>, Geoffroy Sossa<sup>2, 4</sup>, Danica Antonijević<sup>1</sup>, Maren Dubbert<sup>1</sup>, Mathias  
4    Hoffmann<sup>1</sup>

5    <sup>1</sup>Leibniz Center for Agricultural Landscape Research (ZALF), Isotope Biogeochemistry and Gas Fluxes, 15374, Müncheberg,  
6    Germany

7    <sup>2</sup>West African Science Service Centre on Climate Change and Adapted Land Use, University of Sciences, Techniques and  
8    Technologies of Bamako (USTTB), BP E 423, Bamako, Mali

9    <sup>3</sup> Council for Scientific and Industrial Research-Savannah Agricultural Research Institute (CSIR-SARI), 00233, Tamale,  
10    Ghana

11    <sup>4</sup>Laboratory of Hydraulic and Water Control, National Institute of Water, University of Abomey-Calavi, Abomey-Calavi, 01  
12    BP 526 Cotonou, Benin

13

14    *Correspondence to:* Reena Macagga (Reena.Macagga@zalf.de)

15 **Abstract**

16 Mitigating the global climate crisis and its consequences, such as more frequent and severe droughts, is one of the major  
17 challenges for future agriculture. Therefore, identifying land use systems and management practices that reduce greenhouse  
18 gas emissions (GHG) and promote water use efficiency (WUE) is crucial. This however, requires accurate and precise  
19 measurements of carbon dioxide ( $\text{CO}_2$ ) fluxes and evapotranspiration (ET). Despite that, commercial systems to measure  $\text{CO}_2$   
20 and ET fluxes are expensive and thus, often exclude research in ecosystems within the Global South. This is especially true  
21 for research and data of agroecosystems in these areas, which are to date still widely underrepresented. Here, we present a  
22 newly developed, low-cost, non-dispersive infrared (NDIR)-based,  $\text{CO}_2$  and ET flux measurement device (~200 Euro) that  
23 provides reliable, accurate and precise  $\text{CO}_2$  and ET flux measurements in conjunction with manual closed chambers. To  
24 validate the system, laboratory and field validation experiments were performed, testing multiple different low-cost sensors.  
25 We demonstrate that the system delivers accurate and precise  $\text{CO}_2$  and ET flux measurements using the K30 FR NDIR ( $\text{CO}_2$ )  
26 and SHT31 (RH) sensor. An additional field trial application demonstrated its longer-term stability (> 3 months) and ability to  
27 obtain valid net ecosystem C balances (NECB) and WUE. This was the case, even though environmental conditions at the  
28 field trial application site in Sub-Saharan Africa were rather challenging (e.g., extremely high temperatures, humidity and  
29 intense rainfall). Consequently, the developed low-cost  $\text{CO}_2$  and ET flux measurement device does not only provide reasonable  
30 results, but might also help to democratise science and close current data gaps.

31 **1 Introduction**

32 The global climate crisis is one of the most critical problems of our time and identifying and implementing measures to mitigate  
33 or adapt to its consequences, such as more frequent and severe drought, is a key challenge. Solving this challenge, requires  
34 first and foremost a substantial reduction of anthropogenic greenhouse gas (GHG) emissions in all sectors (IPCC, 2019). While  
35 agriculture is a significant contributor to these anthropogenic GHG emissions (FAO, 2020), it might also offer the potential to  
36 mitigate the climate crisis by increasing soil carbon (C) sequestration (Lal et al., 2004). Specifically, land use systems and  
37 management practices which not only promote a net C uptake but also an efficient water use are needed. They might help to  
38 increase soil C stocks and crop productivity, reducing GHG emissions while simultaneously sustaining yield, despite  
39 intensifying climate stressors, such as more frequent and severe droughts. Hence, it is crucial to evaluate land use systems  
40 regarding their potential to sequester additional C and effectively utilize water. Common parameters used to assess both, are  
41 the net ecosystem C balance (NECB; Smith et al., 2010), and the agronomic and ecosystem water use efficiency (WUE; Beer  
42 et al., 2009). Their determination, however, requires accurate and precise measurement of carbon dioxide ( $\text{CO}_2$ ) and  
43 evapotranspiration (ET) fluxes (Chapin et al., 2006; Livingston and Hutchinson, 1995; Rosenstock et al., 2016; Xu et al.,  
44 2019).

46 Measurement of CO<sub>2</sub> and ET fluxes are commonly performed using eddy covariance or chamber based systems (Baldocchi et  
47 al., 1996; Smith et al., 2010; Wang et al., 2017; Yang et al., 2014), while especially the latter are well suited for direct treatment  
48 comparisons (Dubbert et al., 2014; Hoffmann et al., 2018; Kübert et al., 2020). In case of a remote study site location or  
49 limitations in power supply, particularly manual closed chamber measurements are used to measure the CO<sub>2</sub> exchange and ET  
50 fluxes (Rochette and Hutchinson, 2015). However, the relatively high costs of needed measurement equipment (particularly  
51 gas analyzers) strongly limits their accessibility and often exclude research in ecosystems within the Global South. This  
52 resulted in a pronounced underrepresentation of regions, land use systems and management practices from subtropical and  
53 tropical South America, South Asia, and Africa, even though the quantification of e.g., CO<sub>2</sub> fluxes in these regions might  
54 reduce disparities in the global CO<sub>2</sub> budget (Canadell et al., 2011; Gurney et al., 2002; Kondo et al., 2015).

55

56 Recent efforts to solve this financial constraint focus on developing low-cost, yet reliable, measurement devices. This was  
57 catalyzed by the growing availability of relatively inexpensive microcontrollers, which are increasingly utilized for scientific,  
58 environmental research (Blackstock et al., 2019; Capri et al., 2021). An additional contribution came from the improvement  
59 in accuracy and precision of low-cost relative humidity (RH) and especially non-dispersive infrared (NDIR) CO<sub>2</sub> sensors.  
60 Evaluation of commercially-available NDIR CO<sub>2</sub> sensors (Keimel et al., 2019; Martin et al., 2017; Pandey et al., 2007; Yasuda  
61 et al., 2012) showed that they have acceptable precision and accuracy in measuring CO<sub>2</sub> concentrations especially when proper  
62 calibration methods are applied. Although low-cost NDIR CO<sub>2</sub> sensors are commonly used in air quality monitoring studies  
63 (Araújo et al., 2020; Wastine et al., 2022), these sensors have also been applied in environmental research (Bastviken et al.,  
64 2015; Brown et al., 2020). For example, multiple studies have demonstrated the applicability of using low-cost NDIR CO<sub>2</sub>  
65 sensors for reliable measurements of soil CO<sub>2</sub> efflux (Brändle and Kunert, 2019; Curcoll et al., 2022; Harmon et al., 2015) and  
66 water crop use determination (Capri et al., 2021). However, in case of RH sensors, the inversely increased measurement  
67 uncertainty of total water vapor concentration with decreasing RH (e.g. a typical low-cost RH sensor has a measurement  
68 accuracy of 1-3 % in relative but not absolute humidity) might constitute a problem. Despite first studies showing the potential  
69 of using low-cost sensors as an alternative to more expensive commercial counterparts, there is still little evidence that in situ  
70 closed chamber CO<sub>2</sub> and ET flux measurements using both, are comparable in precision and accuracy.

71

72 Here, we present the hard- and software implementation, as well as laboratory and in situ validation of a newly, low-cost and  
73 open-source CO<sub>2</sub> and ET flux measurement device. We hypothesise that by using the device in conjunction with a manual  
74 closed chamber 1.) CO<sub>2</sub> and ET fluxes can be reliably and accurately measured; and that 2.) measured CO<sub>2</sub> and ET fluxes can  
75 be used to obtain valid estimates of net ecosystem C balance (NECB) and WUE, even under challenging environmental  
76 conditions such as extremely high air temperatures, humidity, and precipitation. To test these hypotheses, we first validated  
77 the accuracy and precision of four different low-cost NDIR CO<sub>2</sub> sensors (K30 FR, SCD30, MH-Z14, and MH-Z19) under  
78 controlled laboratory conditions. Afterwards, the NDIR sensors passing laboratory validation as well as two different RH

79 sensors were validated in field. During field validation, ET and CO<sub>2</sub> fluxes (ecosystem respiration (R<sub>eco</sub>) and net ecosystem  
80 exchange (NEE)), as well as temperature-dependent R<sub>eco</sub> and photosynthetic active radiation (PAR)-dependent gross primary  
81 production (GPP) parameters, were compared to the results obtained simultaneously with a reference infrared gas analyser  
82 (IRGA; LI-850, LI-COR, USA). Finally, the ability of the developed low-cost CO<sub>2</sub> and ET flux measurement device to obtain  
83 reliable NECB and WUE as well as its practicability and stability were tested. Therefore, multiple devices were used during a  
84 field trial application in Northern Ghana to obtain seasonal CO<sub>2</sub> exchange and ET, as well as NECB and WUE for four different  
85 fertilizer treatments in a maize cultivation.

86 **2 Material and Methods**

87 **2.1 Hard- and software implementation**

88 The developed, highly portable CO<sub>2</sub> and ET flux measurement device consists of a logger and sensor unit, both assembled out  
89 of a combination of various low-cost, off-the-shelf components. A complete list of used components, distributors and prices is  
90 given in Table 1. Figure 1 shows the assembled logger and attachable sensor unit, together with a schematic representation of  
91 the wiring. The logger unit consists of an Arduino Uno like microcontroller (Atmega328, AZ-Delivery Vertriebs GmbH,  
92 Germany) with attached Logger Shield module (AZ-Delivery Vertriebs GmbH, Germany) including an SD card reader and  
93 SD card (2 GB) to store sensor readings and a real time clock (RTC) which helps to keep the time and date even when the  
94 system is switched off. A BME280 air temperature ( $\pm 1$  °C), air humidity ( $\pm 3$  %) and air pressure sensor ( $\pm 1$  hPa; Reichelt  
95 electronics GmbH, Germany) as well as an LCD display (AZ-Delivery Vertriebs GmbH, Germany) and HC-05 Bluetooth  
96 module are part of the logger unit and connected to the microcontroller. The logger unit is fitted into a weather and shock  
97 resistant outdoor housing (B&W Outdoor Case Type 500, OVERHAUL MEDIA GmbH, Germany). It easily connects to end  
98 user devices using the Bluetooth module, so data can be visualized inter-alia with a smartphone in real-time without the need  
99 to open the weather and shock resistant outdoor housing. The external sensor unit consists of a NDIR-based CO<sub>2</sub> (0-10000  
100 ppm,  $\pm 30$  ppm  $\pm 3$  % accuracy; K30 FR, Senseair AB, Sweden), an air humidity (RH) and air temperature sensor (SHT31,  $\pm 2$   
101 % accuracy, Sensirion AG, Switzerland or DHT22,  $\pm 2$  to 5 % accuracy, Aosong Electronics Co., Ltd, China). Both sensors  
102 were connected through a seven core cable to the logger unit using UART (K30 FR) and I2C (SHT31) data communication,  
103 respectively. The power supply of the microcontroller is ensured by six rechargeable AA NiMH batteries (1.2 V; 2600 mAh)  
104 in a 6×AA battery holder, which supply 7.2 V. Due to the power requirements of the external sensor unit (K30 FR and SHT31),  
105 an additional 6×AA battery holder is attached to the housing directly. Software implementation was done using Arduino IDE  
106 2.0.3.

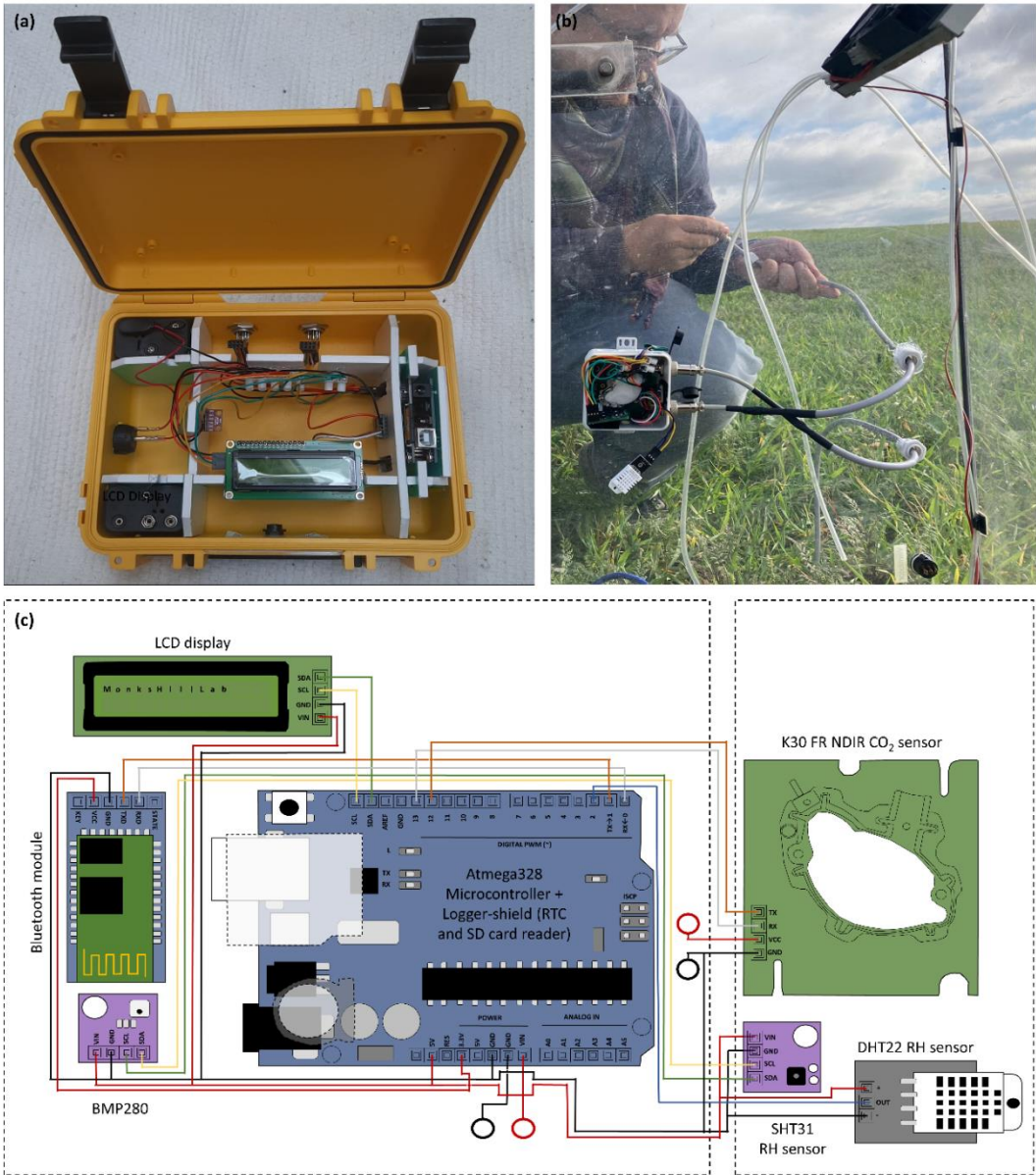
107

108

109

110 **Table 1:** Sensor components and cost (in Euro) at the time of writing, including weather and shock-proof housing and energy  
 111 supply (rechargeable batteries). Components needed for optional semi-automatic mode are listed in addition.

COMPONENT	AMOUNT	DESCRIPTION	PRICE	DISTRIBUTOR
B&W OUTDOOR CASE TYP 500	1	Outdoor case for housing electrical components	28.75 Euro	<a href="http://www.profikoffer.de">www.profikoffer.de</a>
PVC HARD FOAM PLATE	1	PVC 5 mm hard foam plate to create interior of housing for electronic components	1.5 Euro	<a href="http://www.amazon.de">www.amazon.de</a>
LUSTER TERMINALS	12	Luster terminals for wiring electrical components within housing	0.6 Euro	<a href="http://www.amazon.de">www.amazon.de</a>
0.2 MM <sup>2</sup> 24 AWG ELECTRICAL WIRE		Electrical wires for wiring electrical components within housing		<a href="http://www.amazon.de">www.amazon.de</a>
7 PIN AVIATION CONNECTOR	2	Aviation connector to connect logger unit within weatherproof housing with passive NDIR sensor installed in the closed chamber to be attached	2.9 Euro	<a href="http://www.amazon.de">www.amazon.de</a>
7 CORE RUBBER CABLE (1.5 M)	1	Cable to connect logger unit within weatherproof housing with passive NDIR sensor installed in the closed chamber to be attached	3.75 Euro	<a href="http://www.conrad.de">www.conrad.de</a>
WS R13-112 AAAA ROCKER SWITCH	1	Rocker switch for switching on and off	1 Euro	<a href="http://www.reichelt.de">www.reichelt.de</a>
ATMEGA 328	1	Arduino Uno like microcontroller	5 Euro	<a href="http://www.az-delievery.de">www.az-delievery.de</a>
DATALOGGER MODULE	1	Logger shield for Arduino UNO like microcontroller with SD card reader and RTC unit	4.6 Euro	<a href="http://www.az-delievery.de">www.az-delievery.de</a>
HAMA CLASS 4, SD MEMORY CARD, 2 GB, 10 MB/S	1	SD memory card to save sensor readings	6 Euro	<a href="http://www.saturn.de">www.saturn.de</a>
HC-05 BLUETOOTH WIRELESS RF-TRANSCEIVER-MODULE RS232	1	Bluetooth module for wireless communication	5.2 Euro	<a href="http://www.az-delievery.de">www.az-delievery.de</a>
16×2 LCD OR OLED DISPLAY WITH I2C ADAPTER	1	LCD or OLED display for data visualization	3.7 Euro	<a href="http://www.az-delievery.de">www.az-delievery.de</a>
BMP280	1	Air pressure, air humidity and air temperature sensor	1.7 Euro	<a href="http://www.reichelt.de">www.reichelt.de</a>
DHT22 OR SHT31 MODUL	1	Air temperature and air humidity sensor	6.4 Euro	<a href="http://www.az-delievery.de">www.az-delievery.de</a>
SENSEAIR K30 FR (FAST RESPONSE)	1	CO <sub>2</sub> measuring module with fast response time; Measuring range: 0 to 5000 ppm CO <sub>2</sub> , operating range: 0 to 50 °C	85 Euro	<a href="http://www.driessen-kern.de">www.driessen-kern.de</a>
GOOBAY 11467 6× (4×) MIGNON (AA) BATTERY HOLDER	2 (1)	Battery holder for 6× NiMH rechargeable mignon (AA) batteries	4.6 Euro	<a href="http://www.conrad.de">www.conrad.de</a>
CONRAD ENERGY HR06 MIGNON (AA)-AKKU NIMH 2600 MAH 1.2 V	12 (16)	NiMH rechargeable mignon (AA) batteries	38 Euro	<a href="http://www.conrad.de">www.conrad.de</a>
4.5 V METAL BRUSH AIR PUMP	2	Air pump for flushing headspace of small chambers	9.45 Euro	<a href="http://www.berrybase.de">www.berrybase.de</a>
IRLZ44N MOSFET	1	Mosfet to control power supply to pumps	0.75 Euro	<a href="http://www.reichelt.de">www.reichelt.de</a>
<b>COST OF OTHER NDIR SENSORS TESTED</b>				
SENSIRION SCD30 MODULE	1	NDIR gas sensor for CO <sub>2</sub> (0-10000 ppm) integrated with humidity and temperature sensor in the same module	63.50 Euro	<a href="http://www.berrybase.de">www.berrybase.de</a>
MH-Z14 CO <sub>2</sub> SENSOR MODULE	1	NDIR gas sensor for accurately measuring the CO <sub>2</sub> concentration (0-10000 ppm)	55.60 Euro	<a href="http://www.kaufland.de">www.kaufland.de</a>
MH-Z19 CO <sub>2</sub> SENSOR MODULE	1	NDIR gas sensor for accurately measuring the CO <sub>2</sub> concentration (0-10000 ppm)	28.50 Euro	<a href="http://www.reichelt.de">www.reichelt.de</a>
<b>TOTAL COST</b>			<b>199.7 Euro</b>	



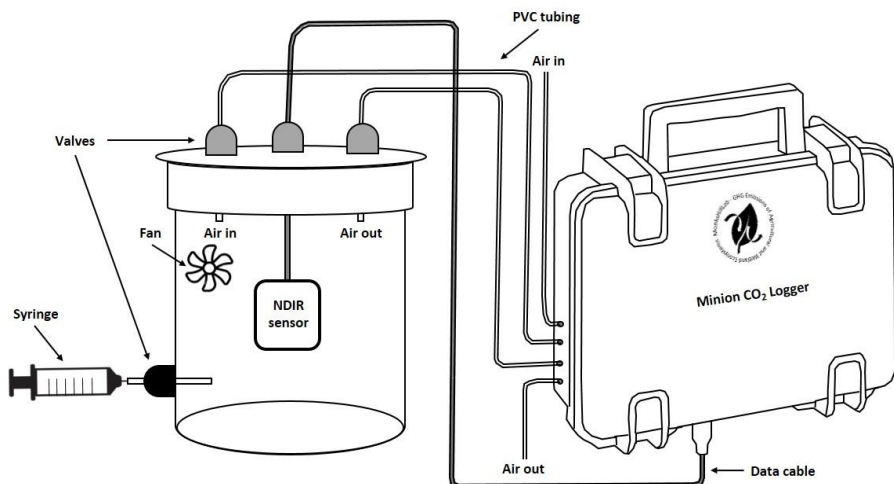
112

113 **Figure 1:** (a) Logger unit in weather and shock resistant housing, (b) external sensor unit attached to a transparent non-flow-  
 114 through non-steady-state (NFT-NSS) closed chamber and (c) schematic representation of wiring.

115 **2.2 Laboratory validation**

116 To identify the NDIR sensor most suitable for in situ, dynamic closed chamber measurements, four different NDIR-based  
117 sensors, were tested and validated regarding their precision and accuracy during a laboratory validation experiment. The  
118 sensors tested were 1.) MH-Z19 (Winsen Electronics Technology CO., LTD, China), 2.) MH-Z14 (Winsen Electronics  
119 Technology CO., LTD, China), 3.) SCD30 (Sensirion AG, Switzerland) and 4.) K30 FR (Senseair AB, Sweden). Sensors were  
120 placed separately into a sealed, ventilated, cylindrical vessel (Fig. 2; V: 1425.5 cm<sup>3</sup>) and connected to the developed low-cost  
121 logger system.

122



123

124 **Figure 2:** Experimental setup of the performed laboratory validation experiment for four different NDIR CO<sub>2</sub> sensors  
125 connected to the developed low-cost CO<sub>2</sub> and ET flux measurement device (MH-Z14, MH-Z19, SCD30 and K30 FR).  
126 Validation was performed through injecting distinct amounts of technical gas (Linde, Germany; 10000 ppm CO<sub>2</sub>) into the air-  
127 tight, sealed, cylindrical vessel.

128 All sensors were calibrated in ambient air prior to use according to manufacturer instructions. Afterwards different distinct  
129 amounts (5 to 30 ml; in 5 ml steps; each step repeated five times) of a technical gas containing 10000 ppm CO<sub>2</sub> (Linde,  
130 Germany) were injected into the sealed vessel using a syringe. In between injections, the vessel was flushed with ambient air  
131 by two pumps (1.5 L min<sup>-1</sup>) connected to the vessel (semi-automatic measurement mode of the developed device). Finally,  
132 CO<sub>2</sub> concentration increases inside the vessel, measured in a 5 s interval by the NDIR-based sensors, from before to after  
133 injection ( $\Delta$ CO<sub>2</sub> in ppm) were compared against mixing-induced CO<sub>2</sub> concentration increases. Sensors that performed best in  
134 terms of accuracy and precision were subsequently validated during the field validation experiment.

135 **2.3 Field validation**

136 Field validation of the low-cost CO<sub>2</sub> and ET flux measurement device was performed through parallel manual closed chamber  
137 measurements using an infrared gas analyzer (IRGA; LI-850, LI-COR, USA) and NDIR sensors (CO<sub>2</sub>) passing previous  
138 laboratory validation, as well as two different RH sensors (ET). Measurements were conducted at the “PatchCrop”  
139 experimental field, managed by the Leibniz Centre for Agricultural Landscape Research (Fig. 3; ZALF). “PatchCrop” features  
140 multiple smaller patches (72 x 72 m), with diverse and site-specific crop rotations, aiming to create synergies and interactions  
141 between fields.



142

143 **Figure 3:** Parallel opaque (R<sub>eco</sub>) manual closed chamber measurements with a LI-COR 850 IRGA (LI-850, LI-COR, USA)  
144 and the developed, low-cost CO<sub>2</sub> and ET flux measurement device at ZALF experimental field near the village of Tempelberg,  
145 North-East Germany (52°26,827' N, 14°8492' E). The developed system was equipped with a K30 FR and SCD30 NDIR, as  
146 well as SHT31 and DHT22 sensor.

147 The experimental field “PatchCrop” is located near the village of Tempelberg, Northeast Germany (52°26,827' N, 14°8492' E). The temperate climate is characterized by a mean annual air temperature of 9.7°C and mean annual precipitation of 544  
148 mm (ZALF weather station, 2010-2019). The medium loamy, sand textured soil can be classified as Luvisol (WRB). CO<sub>2</sub>  
149 exchange (NEE and R<sub>eco</sub>) and ET measurements were conducted for a mixture of *Phacelia* and *Guizotia abyssinica* at three  
150 repetitive plots, established at one of the patches through installing PVC collars (A: 0.5625 m<sup>2</sup>; 5 cm deep) in the beginning  
151 of October 2022. Measurements started shortly after sunrise and lasted to late afternoon during two consecutive days, using a  
152 dynamic, (non-)flow-through non-steady-state ((N)FT-NSS) manual closed chamber system. Used transparent (86 % light  
153 transmission; NEE flux measurements) and opaque (R<sub>eco</sub> flux measurements), cubic shaped PVC chambers had a total volume  
154

155 of 0.296 m<sup>3</sup> and were equipped with a fan for efficient headspace mixing. CO<sub>2</sub> and H<sub>2</sub>O concentrations, as well as RH, during  
156 chamber deployment were recorded in parallel using a LI-850 IRGA and the developed, low-cost measurement device,  
157 equipped with a K30 FR, SCD30, SHT31 and DHT22 sensor, respectively. NEE, R<sub>eco</sub>, and ET fluxes were measured by  
158 alternately deploying the opaque and transparent chambers on the three pre-installed PVC frames. During individual 4 min  
159 measurements, CO<sub>2</sub> and H<sub>2</sub>O concentration changes in the chamber headspace, as well as RH, air temperature inside and  
160 outside the chamber, soil temperature and humidity (TMS-4, TOMST, Czech Republic) as well as PAR (outside the chamber;  
161 Skye, UK) were recorded at a 3 s (LI-850) and 5 s interval (NDIR and RH sensors). To validate the low-cost CO<sub>2</sub> and ET flux  
162 measurement device, measured R<sub>eco</sub>, NEE, and ET fluxes, as well as the derived temperature and PAR dependency functions  
163 for R<sub>eco</sub> and GPP, respectively, were directly compared with results obtained in parallel with the LI-850.

#### 164 **2.4 Field trial application**

165 The developed, low-cost measurement device has been tested for applicability and reliability under challenging environmental  
166 conditions in an experimental field managed by the Council for Scientific and Industrial Research-Savanna Agricultural  
167 Research Institute (Fig. 4; CSIR-SARI). The experimental field (21 × 54 m), located near the city of Nyankpala, Northern  
168 Ghana (9°24'15.9" N, 01°00'12.1" W), featured a split-plot design (3 × 6 m; n=3) with the main plot assigned to tillage  
169 practice (conventional vs. reduced tillage) and the subplot assigned to a factorial combination of organic and mineral fertilizers.  
170 The tropical region around Nyankpala is characterized by a mean annual air temperature of 26 °C and a unimodal rainfall  
171 pattern with a distinct rainy season from June to October followed by a dry season from November to May (Alua et al., 2018)  
172 resulting in a mean annual precipitation of 1100 mm (CSIR-SARI weather station, 1995-2013). The soil is sandy loam textured  
173 and classified as Acrisol (WRB). CO<sub>2</sub> exchange (NEE and R<sub>eco</sub>) and ET measurements were conducted for maize (*Zea mays*)  
174 from July to October 2022 at four out of the nine treatments with reduced tillage (bullock plough), namely: 1.) Fertisoil (5 t  
175 ha<sup>-1</sup>; commercial organic fertilizer in Northern Ghana; FT), 2.) farmyard manure (5 t ha<sup>-1</sup>; FM), 3.) Fertisoil + NPK (5 t ha<sup>-1</sup> +  
176 90-60-60 kg ha<sup>-1</sup>; FT+MIN) and 4.) farmyard manure + NPK (5 t ha<sup>-1</sup> + 90-60-60 kg ha<sup>-1</sup>; FM+MIN). Measurement campaigns  
177 took place every two weeks from sunrise to late evening using a dynamic, NFT-NSS manual closed chamber system. Used  
178 transparent (86 % light transmission; NEE flux measurements) and opaque (R<sub>eco</sub> flux measurements), cubic shaped PVC  
179 chambers had a total volume of 1.56 m<sup>3</sup> and were equipped with a fan for efficient headspace mixing. CO<sub>2</sub> concentration and  
180 RH changes during chamber deployment were recorded using the developed, low-cost measurement device, equipped with a  
181 K30 FR and DHT22 sensor. During each measurement campaign, NEE, R<sub>eco</sub>, and ET fluxes were measured by alternately  
182 deploying the opaque and transparent chambers on pre-installed frames (A: 0.96 m<sup>2</sup>) at each of the measured plots.



184

185 **Figure 4:** Transparent (NEE) manual closed chamber measurement at CSIR-SARI experimental field, used for field trial  
 186 application of the developed, low-cost CO<sub>2</sub> and ET flux measurement device, near the city of Nyankpala, Northern Ghana  
 187 (9°24'15.9'' N, 01°00'12.1'' W).

188 **2.5 Data processing**

189 **2.5.1 CO<sub>2</sub> and ET flux calculation, separation and gap-filling**

190 For laboratory validation, the changes in CO<sub>2</sub> concentrations in the vessel, expressed as  $\Delta\text{CO}_2$  in ppm, were calculated as the  
 191 mixing ratio of measured ambient air and injected technical gas CO<sub>2</sub> concentration (10000 ppm). These were compared with  
 192 the  $\Delta\text{CO}_2$  obtained for the four different NDIR sensors as the difference in mean CO<sub>2</sub> concentrations measured for one minute  
 193 right before and two minutes after injection. For the field validation, measured CO<sub>2</sub> and ET fluxes were calculated using a  
 194 modular R script, described in detail by Hoffmann et al. (2015; CO<sub>2</sub>) and Dahlmann et al. (2023; ET), respectively. Prior to  
 195 CO<sub>2</sub> and ET flux calculation, underlying data was trimmed by removing the first and last 10 % of each chamber measurement  
 196 dataset. This was conducted to eliminate data noise caused by turbulences and pressure fluctuations due to chamber deployment  
 197 (Hoffmann et al., 2015), and to mitigate biases arising from the time needed to homogenize chamber headspace air (Vaidya et  
 198 al., 2021). CO<sub>2</sub> concentrations measured using the LI-850 were additionally corrected for changes in water vapour during  
 199 chamber measurements (Webb et al., 1980; McDermitt et al., 1993). Unlike the LI-850 which provided H<sub>2</sub>O as mole fraction,

200 used low-cost RH sensors (DHT22 and SHT31) required additional post processing. RH measurements were converted into a  
201 mass concentration following Hamel et al. (2015; Eq. 1):  
202

$$203 \quad H_2O = \frac{RH \cdot e^s}{100 \cdot P} \quad (1)$$

204  
205 where RH is the relative humidity, P is the gas pressure (Pa) and  $e^s$  is the saturated vapour pressure (Pa), calculated according  
206 to Allen et al. (1998). Thereafter, CO<sub>2</sub> and ET fluxes were calculated based on the ideal gas law using a linear regression  
207 approach (Eq. 2):  
208

$$209 \quad f = \frac{MpV}{RTA} \cdot \frac{\Delta c}{\Delta t} \quad (2)$$

210  
211 where M denotes the molar mass of the gas (g mol<sup>-1</sup>), p denotes the ambient air pressure (Pa) and V denotes the chamber  
212 volume (m<sup>3</sup>). Since plants accounted for < 0.1 % of the total chamber volume, a static chamber volume was assumed. R denotes  
213 the gas constant (8.314 m<sup>3</sup> Pa K<sup>-1</sup> mol<sup>-1</sup>), T denotes temperature inside the chamber (K), A denotes the basal area (m<sup>-2</sup>) and  
214  $\Delta c/\Delta t$  denotes the linear CO<sub>2</sub> (e.g., Leiber-Sauheitl et al., 2014) and H<sub>2</sub>O concentration change over time (e.g., Dahlmann et  
215 al., 2023). The variables T and, more importantly,  $\Delta c/\Delta t$ , were obtained by applying a variable (window size 0.5 to 4 min)  
216 moving window to each chamber measurement. Thus, resulting multiple ET and CO<sub>2</sub> fluxes per measurement (based on  
217 generated variable moving window data subsets) were further evaluated according to the following criteria: 1.) fulfilled  
218 prerequisites for applying a linear regression (normality (Lilliefor's adaption of the Kolmogorov-Smirnov test),  
219 homoscedasticity (Breusch-Pagan test) and linearity); 2.) regression slope ( $p \leq 0.1$ , t-test); 3.) range of within-chamber air  
220 temperature not larger than  $\pm 1.5$  K and a PAR deviation (only transparent chamber measurements) not larger than  $\pm 20$  % of  
221 the average to ensure stable environmental conditions within the chamber throughout the respective measurement window; 4.)  
222 no outliers present ( $\pm 6 \times IQR$ ). Calculated CO<sub>2</sub> and ET fluxes that did not meet all criteria were discarded. In cases where more  
223 than one flux per measurement met all criteria, the CO<sub>2</sub> and ET flux with the steepest slope and closest in time to chamber  
224 closure were chosen. For field validation and field trial application CO<sub>2</sub> fluxes were additionally separated into its flux  
225 components R<sub>eco</sub>, GPP and NEE and gap-filled through deriving empirical models. In the case of R<sub>eco</sub>, a temperature-dependent  
226 Arrhenius-type function was used and fitted for air as well as soil temperatures measured in different depths (Lloyd and Taylor,  
227 1994; Eq. 3).  
228

$$229 \quad R_{eco} = R_{ref} \cdot e^{E_0 \left[ \frac{1}{T_{ref} - T_0} - \frac{1}{T - T_0} \right]} \quad (3)$$

231 where  $R_{ref}$  is the respiration rate at the reference temperature ( $T_{ref}$ : 283.15 K),  $E_0$  is an activation energy-like parameter,  $T_0$  is  
 232 the starting temperature constant (227.13 K) and  $T$  is the mean air or soil temperature during the flux measurement. Out of the  
 233 four obtained  $R_{eco}$  models (one model for air temperature inside the chamber, one for air temperature outside the chamber; soil  
 234 temperature at 2 and 5 cm depth), the model with the lowest Akaike information criterion (AIC) was finally used. In case of  
 235 GPP a PAR dependent, rectangular hyperbolic light-response function, based on the Michaelis–Menten kinetic, was used  
 236 (Elsgaard et al., 2012; Hoffmann et al., 2015; Wang et al., 2013; Eq. 4). Since GPP cannot be measured directly, GPP fluxes  
 237 were calculated as the difference between measured NEE and modelled  $R_{eco}$  fluxes, using campaign specific, previously  
 238 derived parameters  $R_{ref}$  and  $T_0$ .

$$239 \\ 240 \quad GPP = \frac{GP_{max} \cdot \alpha \cdot PAR}{\alpha \cdot PAR + GP_{max}} \quad (4)$$

241 where  $GP_{max}$  is the maximum rate of C fixation at infinite PAR ( $\mu\text{mol CO}_2 \text{ m}^{-2} \text{ s}^{-1}$ ),  $\alpha$  is the light use efficiency ( $\mu\text{mol CO}_2$   
 242  $\mu\text{mol}^{-1}$  photons) and PAR is the photon flux density (corrected for chamber light transmission) of the photosynthetically active  
 243 radiation ( $\mu\text{mol}^{-1}$  photons  $\text{m}^{-2} \text{ s}^{-1}$ ). In cases where the rectangular hyperbolic light-response function did not result in  
 244 significant parameter estimates, a non-rectangular hyperbolic light-response function was used (Gilmanov et al., 2007; 2013).  
 245  $R_{eco}$  and GPP parameter sets were evaluated and discarded in case of non-significant parameter estimates. If no fit or a non-  
 246 significant fit was achieved, averaged flux rates were used for  $R_{eco}$  and GPP instead.  $R_{eco}$ , GPP and NEE were modelled in half  
 247 hourly steps for the entire period based on continuously monitored temperature and PAR. For ET, campaign-wise average  
 248 daily ET fluxes (for nighttime ET fluxes measured before, for daytime ET fluxes measured after 8:00) were determined and  
 249 linearly interpolated between campaigns for the entire crop growth period.

## 251 2.5.2 NECB and WUE

252 NECB for the field trial application experiment was calculated as the sum of cumulated NEE, C output such as harvested  
 253 biomass C and C input due to organic fertilizer application (Eq. 5; Smith et al., 2010).

$$254 \\ 255 \quad NECB = NEE + C_{input} - C_{output} \quad (5)$$

256 Several minor NECB components have not been considered, such as, C input from seeding and methane emissions. However,  
 257 due to their relatively low magnitude (e.g., no methane emissions in mineral soil under aerobic conditions) their influence on  
 258 the NECB of our study is neglectable. Values for  $R_{eco}$ , GPP, NEE, harvested biomass C and NECB are given using the  
 259 atmospheric sign convention (Ceschia et al., 2010), where positive values indicate C losses from the plant-soil system and  
 260 negative values indicate C uptake. Thus, NECB refers to the total change in below-ground C. WUE was calculated as the  
 261 agricultural WUE (WUE<sub>agro</sub>; Eq. 6; Hatfield and Dold, 2019).

$$264 \quad WUE = \frac{DM}{ET} \quad (6)$$

265  
266 where DM denotes harvested dry biomass in g m<sup>-2</sup> and ET is cumulative evapotranspiration in mm.

### 267 **2.5.3 Error calculation and statistical analysis**

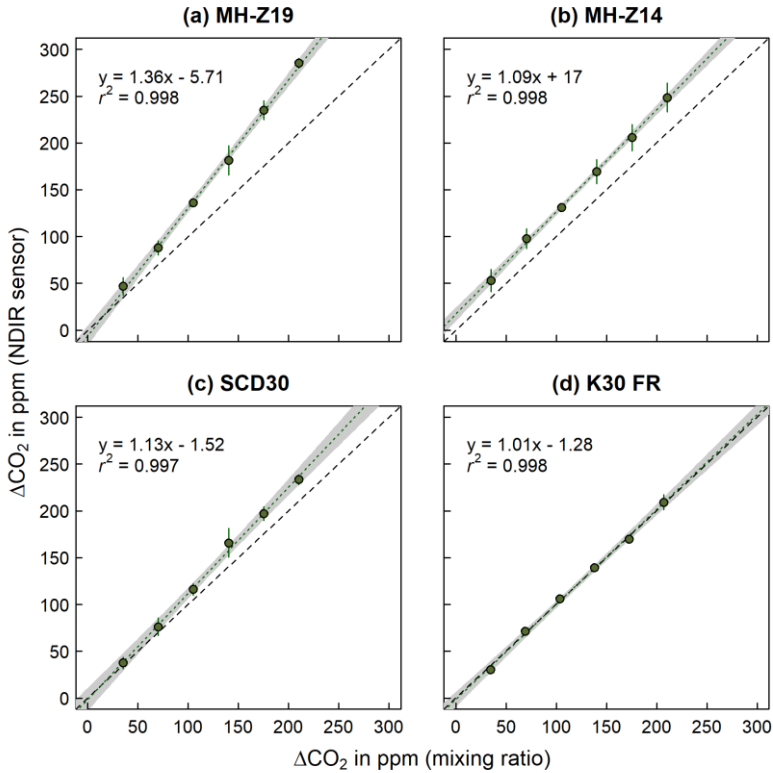
268 To test for normal distribution of the data obtained from laboratory and field validation measurements, Kolmogorov-Smirnov  
269 test ( $p<0.05$ ) was performed. In case of normal distribution, significant differences between  $\Delta CO_2$  in ppm or  $R_{eco}$ , NEE, and  
270 ET fluxes measured from low-cost sensors and mixing ratio  $\Delta CO_2$  or IRGA-based  $R_{eco}$ , NEE, and ET fluxes were determined  
271 using one-sample t-test ( $p<0.05$ ). Error calculation for CO<sub>2</sub> fluxes, as well as crop season CO<sub>2</sub> exchange, were quantified using  
272 a comprehensive error prediction algorithm described in detail by Hoffmann et al. (2015). The approach utilizes bootstrapping  
273 alongside k-fold subsampling to estimate uncertainties for each flux measurement as well as subsequent  $R_{eco}$  and GPP  
274 parametrization and final gap-filling. An adaptation of this approach was used to calculate errors in ET fluxes (Dahlmann et  
275 al., 2023). Seasonal ET flux errors were then estimated based on 1.96×SD of daily average ET fluxes.

## 276 **3 Results and Discussion**

### 277 **3.1 CO<sub>2</sub> sensor laboratory validation**

278 Differences in accuracy and precision among the tested, four different low-cost NDIR sensors are shown in Fig. 5a-d as 1:1-  
279 agreement plots between mixing ratio (calculated) and measured  $\Delta CO_2$ . While accuracy can be assessed as deviation from the  
280 1:1-agreement line, precision is determined by the residual standard deviation (SD) and the coefficient of determination ( $r^2$ )  
281 of the linear regression fitted on calculated versus measured  $\Delta CO_2$ . The K30 FR (Fig. 5d) showed the highest accuracy among  
282 all tested NDIR sensors, reflecting well the increase in CO<sub>2</sub> concentration ( $\Delta CO_2$ ) derived through mixing ratio.  
283 Correspondingly, no significant difference (one sample t-test,  $p=0.80$ ) was found between calculated and measured  $\Delta CO_2$ .  
284 The SCD30 (Fig. 5c), even though fairly accurate at lower, failed to reflect higher calculated  $\Delta CO_2$  values and generally tends  
285 to overestimate triggered  $\Delta CO_2$ . Neither the MH-Z14 (Fig. 5b) nor the MH-Z19 (Fig. 5a) were sufficiently accurate and able  
286 to reflect triggered  $\Delta CO_2$ . While the MH-Z14 showed a rather constant offset from the 1:1-agreement by 28 ppm, the MH-Z19  
287 tends to increasingly overestimate higher  $\Delta CO_2$  values derived through mixing ratio. Hence, unlike the K30 FR, all other NDIR  
288 sensors measured significantly higher  $\Delta CO_2$  when compared to mixing ratio  $\Delta CO_2$  (one sample t-test,  $p<0.01$ ). Unlike the  
289 accuracy, overall precision and measurement repeatability among all four NDIR sensors was generally high and fairly  
290 comparable, showing a residual SD of 2.78 ppm, 4.23 ppm, 2.52 ppm and 3.58 ppm, respectively. Regarding the response time  
291 (defined as mean time from injection to measured initial CO<sub>2</sub> concentration increase), all four NDIR sensors differed  
292 substantially, with only 44 seconds for the K30 FR and more than 280 seconds for the MH-Z14. The same was true for the

293 response strength (defined as the mean time from beginning to end of the injection triggered CO<sub>2</sub> concentration increase, which  
 294 represents its steepness), with 61, 160 and 265 seconds for the K30 FR, SCD30 and MH-Z19 respectively. In case of the MH-  
 295 Z14, response strength could not be evaluated, since no clear saturation after injection induced CO<sub>2</sub> concentration increase  
 296 could be observed.



297  
 298 **Figure 5:** 1:1-agreement between mixing ratio and measured ΔCO<sub>2</sub> in ppm from the four low-cost sensors tested (K30 FR,  
 299 SCD30, MH-Z14 and MH-Z19). The dashed black line indicates the 1:1-agreement. The dotted green line shows the linear  
 300 regression through the average ΔCO<sub>2</sub> for each injection step (n=5), calculated from the repetitive measurements per step. Error  
 301 bars indicate  $\pm 1.96$  SD. The grey shaded area represents the respective confidence band of the regression line.

302 While accuracy and precision are of course highly relevant, response time and response strength in particular play a key role  
 303 in determining the extent to which the tested NDIR sensors can be used for in situ NFT-NSS closed chamber measurements.  
 304 With a response time of almost 2 min and 5 min, respectively, as well as low response strength, MH-Z19 and MH-Z14 would  
 305 likely fail to correctly reflect ΔCO<sub>2</sub> during short-time (<4 min) closed chamber measurements, regardless of their low accuracy,

which makes them additionally unsuitable. Therefore, only the K30 FR (and to a much lower extent the SCD30) with its fast response time and high response strength passed laboratory validation and met all necessary requirements for accurate and precise in situ measurements of CO<sub>2</sub> exchange. Our findings, comparing accuracy and precision of four different NDIR sensors during a laboratory setup, are in a good agreement with previous studies performing laboratory validation of single sensors. Brändle and Kunert (2019), who compared the MH-Z14A NDIR sensor against a GFS-3000 (Heinz Walz GmbH, Germany) during a laboratory validation observed a similar response time and a general measurement offset of approx. +40 ppm. Based on this and an additionally conducted field validation, Brändle and Kunert (2019) also suggested that the MH-Z14A is not suitable for short term measurements (<5 mins). Also findings of González Rivero et al. (2023), who tested the ability of the SCD30 to reflect calibration gas concentrations and concluded an acceptable accuracy and response time, are in a good agreement with results of the present study. The most widely tested NDIR sensors so far, however, are those of the K-Series (as e.g., Ali et al., 2016; Blackstock et al., 2019; Brown et al., 2020; Mendes et al., 2015). Laboratory validation performed by Blackstock et al. (2019) using K30 1 % sensor to measure a span of different CO<sub>2</sub> concentrations verified that it well reflects CO<sub>2</sub> concentrations within the accuracy stated by the manufacturer. Similarly, laboratory tests performed by Mendes et al. (2015) found that the K30 sensor has nearly perfect linear response against calibration gas CO<sub>2</sub> concentrations. Lastly, the laboratory experiment by Ali et al. (2016) also highlighted the accuracy of the K30 1 % sensor when compared against measurements of an SBA-5 CO<sub>2</sub> gas analyzer (PP Systems, USA). During their experiment both sensors showed a strong correlation and no offset, when K30 1 % sensor self-calibration was used, highlighting the self-calibration capabilities of the K-series sensors that contribute to their stable performance and high measurement repeatability with minimal maintenance compared to other NDIR sensors.

### 3.2 Field validation

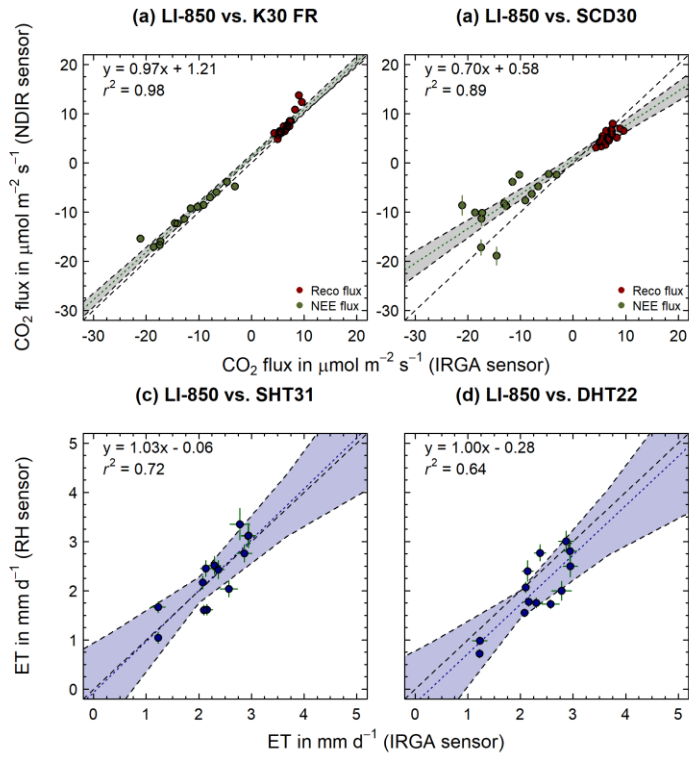
#### 3.2.1. In situ ET flux validation

Two low-cost RH sensors (ET; SHT31 and DHT22) were tested in parallel with NDIR sensors passing the laboratory validation (CO<sub>2</sub>; K30 FR and SCD30) against LI-850 as reference. To avoid systematic impact of opaque chambers on plant transpiration via stomatal closure upon darkening, in case of ET fluxes, only transparent chamber measurements were taken into account (Larcher, 2003). Out of the 20 NEE measurements, 13 valid ET fluxes could be calculated in case of the LI-850. Compared to that, 18 and 17 valid ET fluxes were obtained for the SHT31 and DHT22, respectively. Differences in accuracy and precision for ET fluxes calculated based on RH measurements (Fig. 6c-d) compared to ET fluxes calculated based on LI-850 are shown as 1:1-agreement plots in Fig. 6. No significant difference (mean diff. -0.01 mm d<sup>-1</sup>; one sample t-test,  $p=0.89$ ) was found between ET fluxes calculated from H<sub>2</sub>O concentration and RH measurements, using the LI-850 and SHT31, respectively (Fig. 6c). Together with an  $r^2$  of 0.72, this indicates a reasonable accuracy of SHT31 derived ET flux estimates. Compared to that, ET fluxes, determined through RH measurements using the DHT22 (Fig. 6d), were significantly smaller (mean diff. 0.28 mm

337  $d^{-1}$ ; one sample t-test,  $p < 0.05$ ) than LI-850 based ET fluxes and with an  $r^2$  of 0.64, less accurate. This is consistent with sensor  
338 accuracy for measuring relative humidity specified by their corresponding manufacturers, which are  $\pm 2\%$  accuracy for SHT31  
339 and  $\pm 2-5\%$  accuracy for DHT22. Since these low-cost sensors were only capable of measuring at this level of accuracy, a  
340 higher uncertainty at lower RH concentrations and consequently derived ET fluxes, might occur, even though not directly  
341 detected within this study. The overall precision of SHT31 and DHT22 derived ET fluxes were fairly similar, but with a  
342 residual SD of 0.36 and 0.39  $\text{mm d}^{-1}$ , rather high.

### 343 3.2.2. In situ $\text{CO}_2$ flux validation

344 A total of 41 closed chamber measurements ( $R_{\text{eco}}$ : 21; NEE: 20) has been conducted during the two days field validation, using  
345 the LI-850 as reference for both NDIR sensors passing the laboratory validation ( $\text{CO}_2$ ; K30 FR and SCD30). While for the LI-  
346 850, 41 valid  $\text{CO}_2$  fluxes ( $R_{\text{eco}}$ : 21; NEE: 20) could be calculated, 35 ( $R_{\text{eco}}$ : 21; NEE: 14) and 36 ( $R_{\text{eco}}$ : 21; NEE: 15) valid  
347 fluxes were obtained for K30 FR and SCD30, respectively. Differences in accuracy and precision for  $\text{CO}_2$  fluxes calculated  
348 based on NDIR (Fig. 6a-b) compared to  $\text{CO}_2$  and ET fluxes calculated based on LI-850 are shown as 1:1-agreement plots in  
349 Fig. 6. While the comparison between  $R_{\text{eco}}$  and NEE fluxes calculated from LI-850 and K30 FR measurements (Fig. 6a), was  
350 in accordance with the laboratory validation and showed again the overall accuracy and precision of this NDIR sensor, a small  
351 positive offset was found. Hence,  $\text{CO}_2$  fluxes for the K30 FR were significantly higher ( $R_{\text{eco}}$  mean diff.  $1.12 \mu\text{mol m}^{-2} \text{s}^{-1}$ ; one  
352 sample t-test,  $p < 0.05$ ) and less negative (NEE mean diff.  $1.41 \mu\text{mol m}^{-2} \text{s}^{-1}$ ; one sample t-test,  $p < 0.05$ ) when compared to LI-  
353 850. No such systematic offset was found in case of the SCD30 (Fig. 6b), which showed significantly lower  $R_{\text{eco}}$  (mean diff.  $-1.33 \mu\text{mol m}^{-2} \text{s}^{-1}$ ; one sample t-test,  $p < 0.05$ ) and much less negative NEE fluxes (mean diff.  $-4.18 \mu\text{mol m}^{-2} \text{s}^{-1}$ ; one sample t-  
354 test,  $p < 0.05$ ) compared to LI-850. Since neither both NDIR sensors showed a similar offset, nor an overestimation was found  
355 for the K30 FR during the laboratory validation already, it can be assumed that the detected offset in case of the K30 FR is  
356 neither a direct result of microclimatic effects (e.g., increasing humidity), nor incorrect sensor readings. Instead, inter-alia  
357 differences within the chamber headspace and the position of the NDIR sensor right below the chamber top, approx. 10 cm  
358 above the LI-850 inlet and outlet, might help to explain it. Nonetheless, the NDIR sensor K30 FR still exhibited higher accuracy  
359 than the SCD30 when validated against LI-850 flux measurements. The root mean squared error (RMSE), mean squared error  
360 (MSE), and mean absolute error (MAE) obtained from the K30 FR (RMSE:  $1.77 \mu\text{mol m}^{-2} \text{s}^{-1}$ ; MSE:  $3.16 \mu\text{mol m}^{-2} \text{s}^{-1}$ ; MAE:  
361  $1.34 \mu\text{mol m}^{-2} \text{s}^{-1}$ ) were lower in comparison to SCD30 (RMSE:  $3.97 \mu\text{mol m}^{-2} \text{s}^{-1}$ ; MSE:  $15.77 \mu\text{mol m}^{-2} \text{s}^{-1}$ ; MAE:  $2.80 \mu\text{mol}$   
362  $\text{m}^{-2} \text{s}^{-1}$ ). Compared to the K30 FR, especially NEE fluxes obtained by the SCD30, were also characterized by a very low  
363 precision. The reason for this is certainly the lower  $\text{CO}_2$  concentrations ( $< 400 \text{ ppm}$ ) in the NEE measurements, which are  
364 clearly outside the measurement range specified by the manufacturer (400 to 10000 ppm). This also explains the decreasing  
365 precision with increased negative NEE fluxes obtained by SCD30, since these are likely related to  $\text{CO}_2$  concentration  
366 measurements well below 400 ppm. The general underestimation of  $R_{\text{eco}}$  and NEE fluxes derived from SCD30, however, is  
367 probably a result of its rather long response time and lower response strength when compared to the K30 FR (see 3.1).



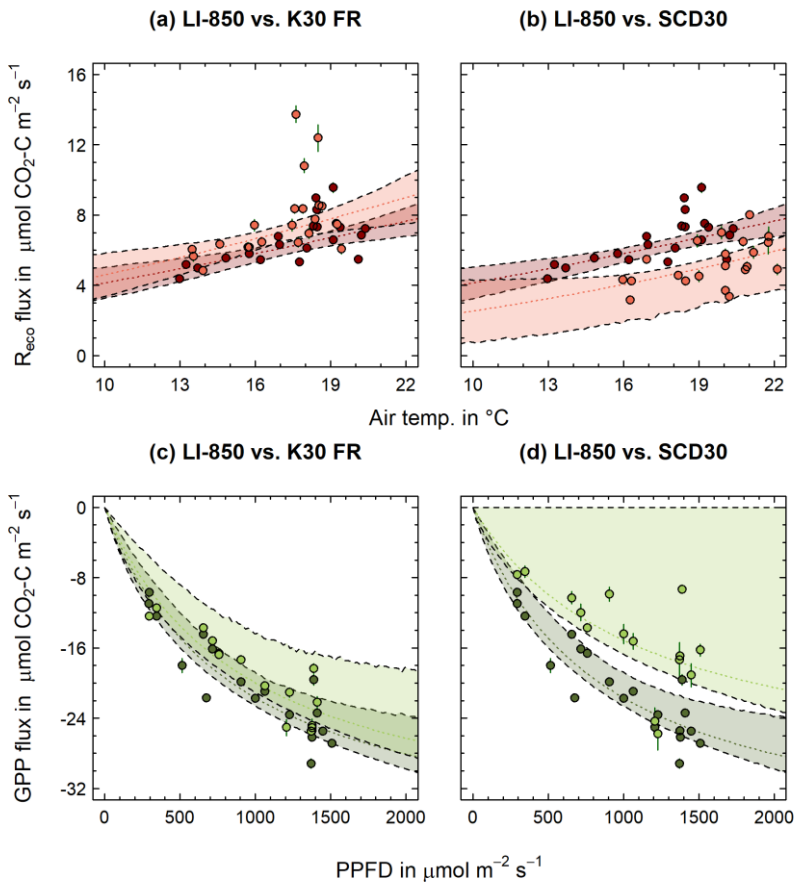
369

370 **Figure 6:** 1:1-agreement between (a-b) CO<sub>2</sub> (R<sub>eco</sub>: dark red points; NEE: dark green points) and (c-d) ET fluxes measured with  
 371 infrared gas analyzer (IRGA; LI-850, LI-COR, USA), and low-cost NDIR sensors (K30 FR and SCD30), as well as low-cost  
 372 RH sensors (SHT 31 and DHT22), respectively. The dashed black line indicates the 1:1-agreement. The dotted green/blue line  
 373 shows the linear regression through the measured CO<sub>2</sub>/ET fluxes. The grey/blue shaded area represents the respective  
 374 confidence band of the regression line. Error bars indicate calculated flux error (CI: 95%;  $p<0.05$ ).

### 375 3.2.3 Temperature- and PAR-dependency of measured CO<sub>2</sub> fluxes

376 Figure 7 shows temperature-dependent R<sub>eco</sub> (Fig. 7a-b) and PAR-dependent GPP (Fig. 7c-d) parameter estimates for flux  
 377 measurements performed with the LI-850 compared to K30 FR (Fig. 7a, 7c) and SCD30 (Fig. 7b, 7d), respectively. Since the  
 378 R<sub>eco</sub> and GPP parameters are based on the fluxes presented in Fig. 6, similar differences between LI-850, K30 FR and SCD30  
 379 could be obtained. With an R<sub>ref</sub> and E<sub>0</sub> of 4.60 and 212.71, the K30 FR had similar, but slightly higher R<sub>eco</sub> parameters (Fig.  
 380 7a) when compared to the LI-850 (R<sub>ref</sub>: 4.14; E<sub>0</sub>: 195.01). This indicates not only in general higher R<sub>eco</sub> fluxes but, more  
 381 importantly, also a stronger increase of R<sub>eco</sub> fluxes with rising temperature. In the case of the SCD30 (R<sub>ref</sub>: 2.54; E<sub>0</sub>: 270.07),

382 differences in  $R_{\text{eco}}$  parameters were, however, much more pronounced. The same tends to be true for obtained GPP parameters,  
383 which were highly comparable for LI-850 ( $\alpha$ : -0.048;  $GP_{\text{max}}$ : -39.83) and K30 FR ( $\alpha$ : -0.042;  $GP_{\text{max}}$ : -38.42), but distinctly  
384 different for SCD30 ( $\alpha$ : -0.029;  $GP_{\text{max}}$ : -31.83). As a result, the fitted K30 FR PAR dependency function was fully within the  
385 confidence band of the LI-850 PAR dependency function. In summary, the K30 FR well represented  $R_{\text{eco}}$  and GPP fluxes  
386 measured with the LI-850 and thereon based parameter estimates for  $R_{\text{eco}}$  and GPP. Unlike the K30 FR, the SCD30 was only  
387 able to reflect LI-850  $R_{\text{eco}}$  and GPP fluxes measured within the manufacture specified concentration range. Correspondingly,  
388 accurate parameter estimates, especially with GPP, were not obtained. Our findings are further supported by studies that  
389 compared the accuracy of K-series sensors against commercial sensor counterparts and its accuracy for field  $\text{CO}_2$  flux  
390 measurements (Curcoll et al., 2022). They integrated a K30 STA sensor into NFT-NSS chamber measurements and were able  
391 to accurately measure  $\text{CO}_2$  fluxes for a grassland ecosystem. Adding to that, the average  $\text{CO}_2$  flux obtained during our study  
392 using K30 FR ( $0.4 \mu\text{mol m}^{-2} \text{s}^{-1}$ ) falls within the range of reported daily average NEE values ( $4$  to  $-6 \mu\text{mol m}^{-2} \text{s}^{-1}$ ) in the study  
393 by Emmel et al. (2018) for a field site in Switzerland which was also covered with *Phacelia* cover crop. Based on the performed  
394 field validation, the developed low-cost measurement device equipped with the K30 FR and SHT31 is likely to accurately  
395 measure  $\text{CO}_2$  and ET fluxes *in situ*, using NFT-NSS closed chambers.



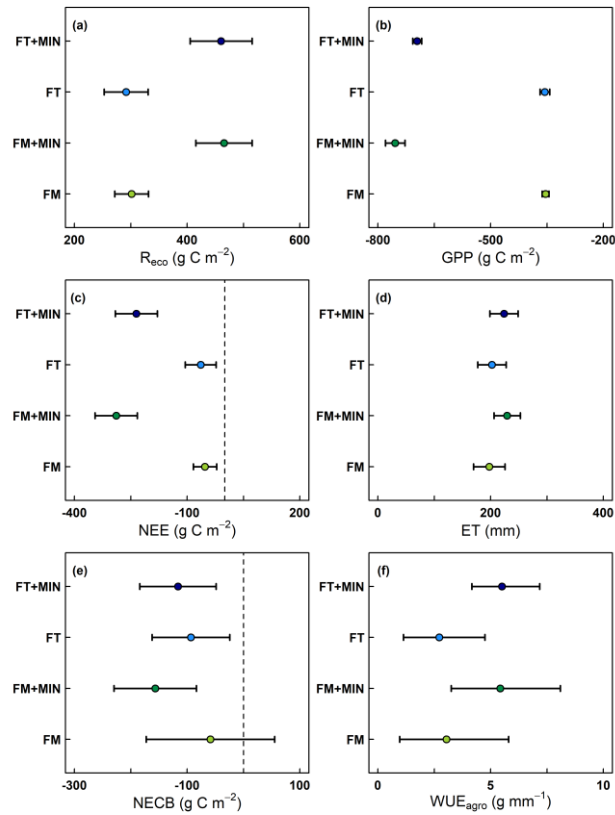
396

397 **Figure 7:** Comparison of R<sub>eco</sub> temperature dependency (dotted red lines) and GPP PAR dependency functions (dotted green lines) between LI-850 (dark red/green) and K30 FR and SCD30 (light red/green), respectively. Shaded red/green areas indicate  
398 confidence band around functions. Dots represent measured R<sub>eco</sub> and derived GPP fluxes. Error bars indicate calculated flux  
399 error (95% CI;  $p < 0.05$ ).  
400

### 401 3.3 Field trial application

402 During the measurement period, half-hourly air temperatures at the field site near Nyankpala, Northern Ghana, reached as high  
403 as 46 °C, with daily average air temperatures ranging from 24 °C to 32 °C. Daily rainfall varied strongly between the rainy  
404 and dry season, with single heavy rain event of up to 115 mm d<sup>-1</sup>. Consequently, average monthly air humidity was highest  
405 (65 to 85 %) during the rainy season and as low as 23 % during the dry season. Irrespective of these harsh environmental

406 conditions, the reliability of the developed low-cost measurement device could be proven during the field trial application.  
407 Periodically performed diurnal CO<sub>2</sub> measurement campaigns resulted in consistent R<sub>eco</sub> and NEE fluxes, showing throughout  
408 the entire crop growth a clear light (PAR) dependency for derived GPP fluxes (data not shown). The maximum daily R<sub>eco</sub> (3.9  
409 g C m<sup>-2</sup> d<sup>-1</sup>) and GPP (-6.9 g C m<sup>-2</sup> d<sup>-1</sup>) fluxes derived for the non-mineral fertilized treatments, were well within the range  
410 (4.0 g C m<sup>-2</sup> d<sup>-1</sup> and -7.0 g C m<sup>-2</sup> d<sup>-1</sup>) of EC derived maximum daily R<sub>eco</sub> and GPP fluxes reported by Quansah et al. (2015),  
411 who measured a mixed fallow and cropping system in Northern Ghana, dominated by tall grasses. When adjusted for  
412 observation length, cumulative NEE, GPP and R<sub>eco</sub> values obtained during the same study (27 g C m<sup>-2</sup>, -195 g C m<sup>-2</sup> and 222  
413 g C m<sup>-2</sup>) were found to be consistent with the average cumulative NEE, GPP and R<sub>eco</sub> values obtained from the non-mineral  
414 fertilized treatments during our field trial application experiment (-58±8 g C m<sup>-2</sup>, -355±1 g C m<sup>-2</sup> and 297±7 g C m<sup>-2</sup>). Also,  
415 EC measurements of an unfertilized cropland system (including maize) in Cameroon resulted with 218.5 g C m<sup>-2</sup> in a  
416 comparable cumulative R<sub>eco</sub> (Verchot et al., 2020). Regarding ET, the highest cumulative ET of our study (FM + MIN; 229±23  
417 mm) was similar to the measured ET flux (238 mm) of a field site in Northern Benin, which was dominated by C4 plants  
418 (Mamadou et al., 2016). In general, obtained cumulative ET (Fig. 8d) for all four treatments were furthermore in a good  
419 agreement with ET obtained for Northern Ghana from average monthly actual evapotranspiration (FAO, 2019), corrected using  
420 phenology specific crop factors for grain maize (263 mm; Brouwer and Heibloem, 1986). Cumulative R<sub>eco</sub> and GPP fluxes  
421 recorded for the four different treatments well-reflected the difference in harvested biomass (529±59 g C m<sup>-2</sup> for FT+MIN and  
422 534±143 g C m<sup>-2</sup> for FM+MIN), with higher cumulative R<sub>eco</sub> and GPP for higher crop biomass (Fig. 8a-b). Consequently, also  
423 NEE and thereon based NECB was higher for additionally, mineral fertilized treatments compared to non-mineral fertilized  
424 treatments, with differences between additionally, mineral and non-mineral fertilized treatments being more pronounced for  
425 FM when compared to FT (Fig. 8c and e). Similar tendencies were found for ET and thereon based WUE, with additionally,  
426 mineral fertilized treatments showing a higher ET and WUE compared to non-mineral fertilized treatments (Fig. 8d and f).  
427 This is in alignment with results reported by Mo et al. (2017) for maize in Kenya, where WUE increased with higher grain  
428 yield due to increasing mineral N fertilization. Besides the reliability of the developed low-cost measurement system, also its  
429 practicability was proved during the field trial application. Despite of the rather demanding environmental conditions, the  
430 system showed that it is uncomplicated and easy to operate even for untrained staff. After a short training session, even non-  
431 technical trained staff can conduct minor repairs of the system directly in the field. However, the missing user interface  
432 currently still prevents direct input of information, such as names of measurement location and soil temperatures, which made  
433 data post processing more tedious.



434

435 **Figure 8:** Cumulative (a-d)  $R_{\text{eco}}$ , GPP, NEE ( $\text{g C m}^{-2}$ ) and ET fluxes (mm) as well as thereon based estimates of (e-f) NECB  
 436 ( $\text{g C m}^{-2}$ ) and WUE ( $\text{g mm}^{-1}$ ) for the four different fertilizer treatments, namely: 1.) Fertisoil ( $5 \text{ t ha}^{-1}$ ; commercial organic  
 437 fertilizer in Northern Ghana; FT), 2.) farmyard manure ( $5 \text{ t ha}^{-1}$ ; FM), 3.) Fertisoil + NPK ( $5 \text{ t ha}^{-1} + 90\text{-}60\text{-}60 \text{ kg ha}^{-1}$ ; FT+MIN)  
 438 and 4.) farmyard manure + NPK ( $5 \text{ t ha}^{-1} + 90\text{-}60\text{-}60 \text{ kg ha}^{-1}$ ; FM+MIN). Error bars indicate calculated flux error (90% CI;  
 439  $p<0.1$ ).

#### 440 4 Conclusions and implications for further use

441 Performed experiments showed that  $\text{CO}_2$  and ET fluxes can be measured reliably and in a stable manner over time using  
 442 inexpensive NDIR and RH sensors in conjunction with a manual closed chamber system. Out of the various low-cost  $\text{CO}_2$  and  
 443 RH sensors that were validated, the K30 FR and SHT31 proved to be the most accurate in measuring  $\text{CO}_2$  and ET fluxes,  
 444 respectively. Additionally, the developed low-cost measurement device was shown to be both practical and applicable to use  
 445 even in environmentally challenging agroecosystems, as demonstrated by the field trial application in Northern Ghana, sub-

446 Saharan Africa. There within, seasonal CO<sub>2</sub> and ET fluxes turned out to be reliable and could be used to obtain valid NECB  
447 and WUE estimates. Since the system developed is battery-powered (solar rechargeable), based on open-source technology  
448 and all its components are low-cost, it can become easily accessible to a broad range of researchers. Its light-weight and low  
449 power consumption with the 12 rechargeable NiMH batteries lasting for as long as eight hours, make the system especially  
450 suitable for in situ closed chamber measurements in remote tropical areas. Compared to Li-ion batteries, the rechargeable  
451 NiMH batteries are furthermore relatively safe to use at high temperatures. This opens manyfold potential applications,  
452 especially in the Global South, regarding the evaluation and identification of various land use systems and management  
453 practices, in terms of their C sequestration potential, water consumption and WUE. Therefore, the developed measurement  
454 device can be a valuable tool in evaluating and assessing global carbon and water flux models, ultimately expanding the  
455 network for C budget and evapotranspiration research that are both critical for climate crisis adaptation and mitigation.

## 456 **5 Data and code availability**

457 The data and code referred to in this study are publicly accessible at <https://doi.org/10.4228/zalf-hdqh-br42>.

## 458 **6 Author contribution**

459 MH and RM conceptualized and developed the system and code. RM, DA and GS carried out the laboratory and field validation  
460 experiments. MA conducted the field trial application. RM, MH, and MD wrote and prepared the manuscript with contributions  
461 of all co-authors. All authors have reviewed and agreed to the final version of the manuscript.

## 462 **7 Competing interests**

463 The authors declare that they have no conflict of interest.

464

## 465 **8 Acknowledgements:**

466 This work was funded by a grant (2819DOKA06) from the German Federal Ministry of Food and Agriculture (BMEL).  
467 Michael Asante and Geoffroy Sossa were supported by the West African Science Service Center on Climate Change and  
468 Adapted Land Use (WASCAL) and the Prince Albert II of Monaco Foundation. The maintenance of the “PatchCrop”  
469 infrastructure is supported by the Leibniz Centre for Agricultural Landscape Research (ZALF). We would also like to extend  
470 our deepest gratitude to Matthias Lueck and Shukrona Giyasidinova for assisting during the laboratory validation experiment,  
471 as well as Shrijana Vaidya and Isabel Zentgraf for helping during the field validation experiment. Special thanks goes to  
472 Ayertey Aquinas Kofi, Mavis Nartey, Narkey Kofi Mark and Abdul-Fataw Alhassan who helped during the field trial  
473 application.

474 **9 References**

475 Ali, A. S., Zanzinger, Z., Debose, D., and Stephens, B.: Open Source Building Science Sensors (OSBSS): A low-cost Arduino-  
476 based platform for long-term indoor environmental data collection, *Building and Environment*, 100, 114–126,  
477 <https://doi.org/10.1016/j.buildenv.2016.02.010>, 2016.

478 Allen, R.G., Pereira, L.S., Raes, D., Smith, M.: Crop evapotranspiration —guidelines for computing crop water requirements,  
479 FAO Irrigation and drainage paper 56, Food and Agriculture Organization, Rome, 1998.

480 Alua, M.A., Peprah, K. and Achana, G.T.W.: Climate change implications for crop farming in Ghana's semi-arid guinea  
481 savanna, *International Journal of Development and Sustainability*, Vol. 7 No. 9, pp. 2334-2349, 2018.

482 Araújo, T., Silva L. T., Moreira A. J. C.: Evaluation of Low-Cost Sensors for Weather and Carbon Dioxide Monitoring in  
483 Internet of Things Context, *MDPI - IoT* 2020, Vol. 1, Issue II, pp. 286-308, <https://doi.org/10.3390/iot1020017>,  
484 2020.

485 Baldocchi, D., Valentini, R., Running, S., Oechel, W., and Dahlman, R.: Strategies for measuring and modelling carbon  
486 dioxide and water vapour fluxes over terrestrial ecosystems, *Global Change Biol*, 2, 159–168, <https://doi.org/10.1111/j.1365-2486.1996.tb00069.x>, 1996.

488 Bastviken, D., Sundgren, I., Natchimuthu, S., Reyier, H., and Gålfalk, M.: Technical Note: Cost-efficient approaches to  
489 measure carbon dioxide (CO<sub>2</sub>) fluxes and concentrations in terrestrial and aquatic environments using mini loggers,  
490 *Biogeosciences*, 12, 3849–3859, <https://doi.org/10.5194/bg-12-3849-2015>, 2015.

491 Beer, C., Ciais, P., Reichstein, M., Baldocchi, D., Law, B., Papale, D., Soussana, J.-F., Ammann, C., Buchmann, N., Frank,  
492 D., Gianelle, D., Janssens, I., Knohl, A., Köstner, B., Moors, E., Roupsard, O., Verbeeck, H., Vesala, T., Williams, C., and  
493 Wohlfahrt, G.: Temporal and among-site variability of inherent water use efficiency at the ecosystem level, *Global  
494 Biogeochemical Cycles*, v.23, GB2018-GB2018 (2009), 2009.

495 Blackstock, J. M., Covington, M. D., Perne, M., and Myre, J. M.: Monitoring Atmospheric, Soil, and Dissolved CO<sub>2</sub> Using a  
496 Low-Cost, Arduino Monitoring Platform (CO2-LAMP): Theory, Fabrication, and Operation, *Front. Earth Sci.*, 7, 313,  
497 <https://doi.org/10.3389/feart.2019.00313>, 2019.

498 Brändle, J. and Kunert, N.: A new automated stem CO<sub>2</sub> efflux chamber based on industrial ultra-low-cost sensors, *Tree  
499 Physiology*, tpz104, <https://doi.org/10.1093/treephys/tpz104>, 2019.

500 Brouwer, C. and Heibloem, M.: Irrigation Water Management: Irrigation Water Needs. Training manual no. 3, Food and  
501 Agriculture Organization of the United Nations, Rome, 1986.

502 Brown, S. L., Goulsbra, C. S., Evans, M. G., Heath, T., and Shuttleworth, E.: Low cost CO<sub>2</sub> sensing: A simple microcontroller  
503 approach with calibration and field use, *HardwareX*, 8, e00136, <https://doi.org/10.1016/j.hx.2020.e00136>, 2020.

504 Canadell, J. G., Ciais, P., Gurney, K., Le Quer' e, C., Piao, S., Rau-pach, M. R., and Sabine, C. L.: An international effort to  
505 quantify regional carbon fluxes, *EOS*, 92, 81–82, 2011.

506 Capri, C., Gatti, M., Guadagna, P., Zozzo, F. D., Magnanini, E., and Poni, S.: A low-cost portable chamber based on Arduino  
507 micro-controller for measuring cover crops water use, *Computers and Electronics in Agriculture*, 190, 106361,  
508 <https://doi.org/10.1016/j.compag.2021.106361>, 2021.

509 Chapin, F. S., Woodwell, G. M., Randerson, J. T., Rastetter, E. B., Lovett, G. M., Baldocchi, D. A., Clark, M. E., Harmon, D.  
510 Schimel, R., Valentini, C., Wirth, J. D. , Aber, J. J., Cole, M. L., Goulden, J. W., Harden, M., Heimann, R. W., Howarth,  
511 P. A., Matson, A. D., McGuire, J. M., Melillo, H. A., Mooney, J. C., Neff, R. A., Houghton, M. L., Pace, M. G., Ryan, S. W.,  
512 Running, O. E., Sala, W. H., Schulze E.D.: Reconciling Carbon-cycle Concepts, Terminology, and Methods. *Ecosystems*,  
513 9(7), 1041–1050, <https://doi:10.1007/s10021-005-0105-7>, 2006.

514 Curcoll, R., Morguí, J.A., Kamnang, A., Cañas, L., Vargas, A., Grossi, C.: Metrology for low-cost CO<sub>2</sub> sensors applications:  
515 the case of a steady-state through-flow (SS-TF) chamber for CO<sub>2</sub> fluxes observations, *Atmos. Meas. Tech.*, 15, 2807–  
516 2818, <https://doi.org/10.5194/amt-15-2807-2022>, 2022.

517 Ceschia, E., Béziat, P., Dejoux, J.-F., Aubinet, M., Bernhofer, C., Bodson, B., Buchmann, N., Carrara, A., Cellier, P., Tommasi,  
518 P., Elbers, J., Eugster, W., Grünwald, T., Jacobs, C., Jans, W., Jones, M., Kutsch, W. L., Lanigan, G., Magliulo, V., and  
519 Wattenbach, M.: Management effects on net ecosystem carbon and GHG budgets at European crop sites, *Agriculture  
520 Ecosystems & Environment*, v.139, 363-383 (2010), 2010.

521 Dahlmann, A., Hoffmann, M., Verch, G., Schmidt, M., Sommer, M., Augustin, J., and Dubbert, M.: Benefits of a robotic  
522 chamber system for determining evapotranspiration in an erosion-affected, heterogeneous cropland, *Hydrology and Earth  
523 System Sciences*, 27, 3851–3873, <https://doi.org/10.5194/hess-27-3851-2023>, 2023.

524 Dubbert, M., Cuntz, M., Piayda, A., and Werner, C.: Oxygen isotope signatures of transpired water vapor: the role of isotopic  
525 non-steady-state transpiration under natural conditions, *New Phytol*, 203, 1242–1252, <https://doi.org/10.1111/nph.12878>,  
526 2014.

527 Elsgaard, L., Görres, C., Hoffmann, C.C., Blicher-Mathiesen, G., Schelde, K., Petersen, S.O.: Net ecosystem exchange of CO<sub>2</sub>  
528 and carbon balance for eight temperate organic soils under agricultural management. *Agric. Ecosyst. Environ.* 162, 52–67,  
529 <https://doi.org/10.1016/j.agee.2012.09.001>, 2012.

530 Emmel, C., Winkler, A., Hörtnagl, L., Revill, A., Ammann, C., D'Odorico, P., Buchmann, N., and Eugster, W.: Integrated  
531 management of a Swiss cropland is not sufficient to preserve its soil carbon pool in the long term, *Biogeosciences*, 15, 5377–  
532 5393, <https://doi.org/10.5194/bg-15-5377-2018>, 2018.

533 FAO-Food and Agriculture Organization: WaPOR v2.1: Water Productivity Open Access Portal (Version 2.1) [Data set],  
534 <http://wapor.apps.fao.org/>, 2019.

535 FAO-Food and Agricultural Organization: Emissions due to agriculture. Global, regional and country trends 2000–2018.  
536 FAOSTAT Analytical Brief Series No. 18, Food and Agriculture Organization of the United Nations, Rome, 2020.

537 Gilmanov, T. G., Soussana, J. F., Aires, L., Allard, V., Ammann, C., Balzarolo, M., Barcza, Z., Bernhofer, C., Campbell, C.  
538 L., Cernusca, A., Cescatti, A., Clifton-Brown, J., Dirks, B. O. M., Dore, S., Eugster, W., Fuhrer, J., Gimeno, C., Gruenwald,  
539 T., Haszpra, L., Hensen, A., Ibrom, A., Jacobs, A. F. G., Jones, M. B., Lanigan, G., Laurila, T., Lohila, A., G. Manca, Marcolla,  
540 B., Nagy, Z., Pilegaard, K., Pinter, K., Pio, C., Raschi, A., Rogiers, N., Sanz, M. J., Stefani, P., Sutton, M., Tuba, Z., Valentini,  
541 R., Williams, M. L., and Wohlfahrt, G.: Partitioning European grassland net ecosystem CO<sub>2</sub> exchange into gross primary  
542 productivity and ecosystem respiration using light response function analysis, *Agriculture, Ecosystems & Environment*, 121,  
543 93–120, <https://doi.org/10.1016/j.agee.2006.12.008>, 2007.

544 Gilmanov, T.G., Wylie, B.K., Tieszen, L.L., Meyers, T.P., Baron, V.S., Bernacchi, C.J., Billesbach, D.P., Burba, G.G., Fischer,  
545 M.L., Glenn, A.J., Hanan, N.P., Hatfield, J.L., Heuer, M.W., Hollinger, S.E., Howard, D.M., Matamala, R., Prueger, J.H.,  
546 Tenuta, M., Young, D.G.: CO<sub>2</sub> uptake and ecophysiological parameters of the grain crops of midcontinent North America:  
547 estimates from flux tower measurements. *Agric, Ecosyst Environ.* 164, 162–175, <https://doi.org/10.1016/j.agee.2012.09.017>,  
548 2013.

549 González Rivero, R. A., Morera Hernández, L. E., Schalm, O., Hernández Rodríguez, E., Alejo Sánchez, D., Morales Pérez,  
550 M. C., Nuñez Caraballo, V., Jacobs, W., and Martínez Laguardia, A.: A Low-Cost Calibration Method for Temperature,  
551 Relative Humidity, and Carbon Dioxide Sensors Used in Air Quality Monitoring Systems, *Atmosphere*, 14, 191,  
552 <https://doi.org/10.3390/atmos14020191>, 2023.

553 Gurney, K. R., Law, R. M., Denning, A. S., Rayner, P. J., Baker, D., Bousquet, P., Bruhwiler, L., Chen, Y.-H., Ciais, P., Fan,  
554 S., Fung, I. Y., Gloor, M., Heimann, M., Higuchi, K., John, J., Maki, T., Maksyutov, S., Masarie, K., Peylin, P., Prather, M.,

555 Pak, B. C., Randerson, J., Sarmiento, J., Taguchi, S., Takahashi, T., and Yuen, C.-W.: Towards robust regional estimates of  
556 CO<sub>2</sub> sources and sinks using atmospheric transport models, *Nature*, 415, 626– 630, 2002.

557 Hamel, P., Mchugh, I., Coutts, A., Daly, E., Beringer, J., and Fletcher, T. D.: Automated Chamber System to Measure Field  
558 Evapotranspiration Rates, *J. Hydrol. Eng.*, 20, 04014037, [https://doi.org/10.1061/\(ASCE\)HE.1943-5584.0001006](https://doi.org/10.1061/(ASCE)HE.1943-5584.0001006), 2015.

559 Harmon, T. C., Dierick, D., Trahan, N., Allen, M. F., Rundel, P. W., Oberbauer, S. F., Schwendenmann, L., and Zelikova, T.  
560 J.: Low-cost soil CO<sub>2</sub> efflux and point concentration sensing systems for terrestrial ecology applications, *Methods Ecol Evol*,  
561 6, 1358–1362, <https://doi.org/10.1111/2041-210X.12426>, 2015.

562 Hatfield, J. L. and Dold, C.: Water-Use Efficiency: Advances and Challenges in a Changing Climate, *Front. Plant Sci.*, 10,  
563 103, <https://doi.org/10.3389/fpls.2019.00103>, 2019.

564 Hoffmann, M., Jurisch, N., Albiac Borraz, E., Hagemann, U., Drösler, M., Sommer, M., Augustin, J.: Automated modeling of  
565 ecosystem CO<sub>2</sub> fluxes based on periodic closed chamber measurements: a standardized conceptual and practical approach,  
566 *Agric. For. Meteorol.* 200, 30–45, <https://doi.org/10.1016/j.agrformet.2014.09.005>, 2015.

567 Hoffmann, M., Pohl, M., Jurisch, N., Prescher, A.-K., Mendez Campa, E., Hagemann, U., Remus, R., Verch, G., Sommer, M.,  
568 and Augustin, J.: Maize carbon dynamics are driven by soil erosion state and plant phenology rather than nitrogen fertilization  
569 form, *Soil and Tillage Research*, 175, 255–266, <https://doi.org/10.1016/j.still.2017.09.004>, 2018.

570 IPCC: P.R. Shukla, J. Skea, E. Calvo Buendia, V. Masson-Delmotte, H.-O. Pörtner, D. C. Roberts, P. Zhai, R. Slade, S.  
571 Connors, R. van Diemen, M. Ferrat, E. Haughey, S. Luz, S. Neogi, M. Pathak, J. Petzold, J. Portugal Pereira, P. Vyas, E.  
572 Huntley, K. Kissick, M. Belkacemi, J. Malley, (eds.): 2019: Climate Change and Land: an IPCC special report on climate  
573 change, desertification, land degradation, sustainable land management, food security, and greenhouse gas fluxes in terrestrial  
574 ecosystems [In press], 2019.

575 IUSS Working Group WRB: World reference base for soil resources 2014. International soil classification system for naming  
576 soils and creating legends for soil maps, *World Soil Resources Reports No. 106*. FAO, Rome, 2015.

577 Keimel, A.: Comparison of Low-Cost CO<sub>2</sub> Non-Dispersive Infrared (NDIR) Sensors for Ambient Greenhouse Gas  
578 Monitoring", UVM Honors College Senior Theses. 282, <https://scholarworks.uvm.edu/hcoltheses/282>, 2019.

579 Kondo, M., K. Ichii, H. Takagi, and Sasakawa, M.: Comparison of the data-driven top-down and bottom-up global terrestrial  
580 CO<sub>2</sub> exchanges: GOSAT CO<sub>2</sub> inversion and empirical eddy flux upscaling, *J. Geophys. Res. Biogeosci.*, 120, 1226–1245,  
581 doi:10.1002/ 2014JG002866, 2015.

582 Kübert, A., Paulus, S., Dahlmann, A., Werner, C., Rothfuss, Y., Orlowski, N., Dubbert, M.: Water Stable Isotopes in  
583 Ecohydrological Field Research: Comparison Between In Situ and Destructive Monitoring Methods to Determine Soil Water  
584 Isotopic Signatures. *Front. Plant Sci.*, 11, 387. DOI: 10.3389/fpls.2020.00387, 2020.

585 Lal, R.: Soil carbon sequestration to mitigate climate change, *Geoderma*, 123, 1–22,  
586 <https://doi.org/10.1016/j.geoderma.2004.01.032>, 2004.

587 Larcher, W.: *Physiological Plant Ecology: Ecophysiology and Stress Physiology of Functional Groups*, 4th ed., Springer  
588 Berlin, Heidelberg, 514 pp., 2003.

589 Leiber-Sauheitl, K., Fuß, R., Voigt, C., and Freibauer, A.: High CO<sub>2</sub> fluxes from grassland on histic Gleysol along soil carbon  
590 and drainage gradients, *Biogeosciences*, 11, 749–761, <https://doi.org/10.5194/bg-11-749-2014>, 2014.

591 Livingston, G.P. and Hutchinson, G.L.: Enclosure-based measurement of trace gas exchange: applications and sources of error,  
592 In Matson, P.A., Harris, R.C. (Eds.), *Methods in Ecology. Biogenic Trace Gases: Measuring Emissions from Soil and Water*,  
593 Blackwell Sci, New York, pp. 14–51, 1995.

594 Lloyd, J. and Taylor, J.A.: On the temperature dependence of soil respiration, *Functional Ecol.* 8, 315–323,  
595 <https://doi.org/10.2307/2389824>, 1994.

596 Mamadou, O., Galle, S., Cohard, J., Peugeot, C., Kounouhewa, B., Biron, R., Hector, B., and Zannou, A. B.: Dynamics of  
597 water vapor and energy exchanges above two contrasting Sudanian climate ecosystems in Northern Benin (West Africa), *JGR  
598 Atmospheres*, 121, <https://doi.org/10.1002/2016JD024749>, 2016.

599 Martin, C. R., Zeng, N., Karion, A., Dickerson, R. R., Ren, X., Turpie, B. N., and Weber, K. J.: Evaluation and environmental  
600 correction of ambient CO<sub>2</sub> measurements from a low-cost NDIR sensor, *Atmos. Meas. Tech.*, 10, 2383–2395,  
601 <https://doi.org/10.5194/amt-10-2383-2017>, 2017.

602 McDermitt, D. K., Welles J. M., Eckles R. D.: Effects of temperature, pressure and water vapor on gas phase infrared  
603 absorption by CO<sub>2</sub>. LI-COR Biosciences Inc. 1993.

604 Mendes, L., Ogink, N., Edouard, N., van Dooren, H., Tinôco, I., and Mosquera, J.: NDIR Gas Sensor for Spatial Monitoring  
605 of Carbon Dioxide Concentrations in Naturally Ventilated Livestock Buildings, *Sensors*, 15, 11239–11257,  
606 <https://doi.org/10.3390/s150511239>, 2015.

607 Mo, F., Wang, J.-Y., Zhou, H., Luo, C.-L., Zhang, X.-F., Li, X.-Y., Li, F.-M., Xiong, L.-B., Kavagi, L., Nguluu, S. N., and  
608 Xiong, Y.-C.: Ridge-furrow plastic-mulching with balanced fertilization in rainfed maize (*Zea mays* L.): An adaptive  
609 management in east African Plateau, Agricultural and Forest Meteorology, 236, 100–112,  
610 <https://doi.org/10.1016/j.agrformet.2017.01.014>, 2017.

611 Pandey, S., Kim, K.H., Lee, S.H.: Use of a Dynamic Enclosure Approach to Test the Accuracy of the NDIR Sensor: Evaluation  
612 Based on the CO<sub>2</sub> Equilibration Pattern. Sensors, 7(12), 3459–3471, <https://doi:10.3390/s7123459>, 2007.

613 Quansah, E., Mauder, M., Balogun, A. A., Amekudzi, L. K., Hingerl, L., Bliefernicht, J., and Kunstmann, H.: Carbon dioxide  
614 fluxes from contrasting ecosystems in the Sudanian Savanna in West Africa, Carbon Balance Manage, 10, 1,  
615 <https://doi.org/10.1186/s13021-014-0011-4>, 2015.

616 Rochette, P. and Hutchinson, G. L.: Measurement of Soil Respiration in situ: Chamber Techniques, in: Agronomy  
617 Monographs, edited by: Hatfield, J. L. and Baker, J. M., American Society of Agronomy, Crop Science Society of America,  
618 and Soil Science Society of America, Madison, WI, USA, 247–286, <https://doi.org/10.2134/agronmonogr47.c12>, 2015.

619 Rosenstock, T. S., Mpanda, M., Pelster, D. E., Butterbach-Bahl, K., Rufino, M. C., Thiong'o, M., Mutuo, P., Abwanda, S.,  
620 Rioux, J., Kimaro, A.A., Neufeldt, H.: Greenhouse gas fluxes from agricultural soils of Kenya and Tanzania. Journal of  
621 Geophysical Research: Biogeosciences, 121(6), 1568–1580, <https://doi:10.1002/2016jg003341>, 2016.

622 Smith, P., Lanigan, G., Kutsch, W. L., Buchmann, N., Eugster, W., Aubinet, M., Ceschia, E., Béziat, P., Yeluripati, J. B.,  
623 Osborne, B., Moors, E. J., Brut, A., Wattenbach, M., Saunders, M., and Jones, M.: Measurements necessary for assessing the  
624 net ecosystem carbon budget of croplands, Agriculture, Ecosystems & Environment, 139, 302–315,  
625 <https://doi.org/10.1016/j.agee.2010.04.004>, 2010.

626 Vaidya, S., Schmidt, M., Rakowski, P., Bonk, N., Verch, G., Augustin, J., Sommer, M., and Hoffmann, M.: A novel robotic  
627 chamber system allowing to accurately and precisely determine spatio-temporal CO<sub>2</sub> flux dynamics of heterogeneous  
628 croplands, Agricultural and Forest Meteorology, 296, 108206, <https://doi.org/10.1016/j.agrformet.2020.108206>, 2021.

629 Verchot, L. V., Dannenmann, M., Kengdo, S. K., Njine-Bememba, C. B., Rufino, M. C., Sonwa, D. J., and Tejedor, J.: Land-  
630 use change and Biogeochemical controls of soil CO<sub>2</sub>, N<sub>2</sub>O and CH<sub>4</sub> fluxes in Cameroonian forest landscapes, Journal of  
631 Integrative Environmental Sciences, 17, 45–67, <https://doi.org/10.1080/1943815X.2020.1779092>, 2020.

632 Wang, K., Liu, C., Zheng, X., Pihlaite, M., Li, B., Haapanala, S., Vesala, T., Liu, H., Wang, Y., Liu, G., Hu, F.: Comparison  
633 between eddy covariance and automatic chamber techniques for measuring net ecosystem exchange of C dioxide in cotton and  
634 wheat fields, Biogeosciences 10, 6865–6877, <https://doi.org/10.5194/bg-10-6865-2013>, 2013.

635 Wang, X., Wang, C., and Bond-Lamberty, B.: Quantifying and reducing the differences in forest CO<sub>2</sub>-fluxes estimated by  
636 eddy covariance, biometric and chamber methods: A global synthesis, *Agricultural and Forest Meteorology*, 247, 93–103,  
637 <https://doi.org/10.1016/j.agrformet.2017.07.023>, 2017.

638 Wastine, B., Hummelgård, C., Bryzgalov, M., Rödjemård, H., Martin, H., Schröder, S.: Compact Non-Dispersive Infrared  
639 Multi-Gas Sensing Platform for Large Scale Deployment with Sub-ppm Resolution. *Atmosphere*, 13, 1789.  
640 <https://doi.org/10.3390/atmos13111789>, 2022.

641 Webb, E. K., Pearman, G. I., & Leuning, R.: Correction of flux measurements for density effects due to heat and water vapour  
642 transfer, *Quarterly Journal of the Royal Meteorological Society*, 106(447), 85–100, <https://doi.org/10.1002/qj.49710644707>,  
643 1980.

644 Xu, C., McDowell, N. G., Fisher, R. A., Wei, L., Sevanto, S., Christoffersen, B. O., Weng, E., and Middleton, R. S.: Increasing  
645 impacts of extreme droughts on vegetation productivity under climate change, *Nat. Clim. Chang.*, 9, 948–953,  
646 <https://doi.org/10.1038/s41558-019-0630-6>, 2019.

647 Yang, F., Zhang, Q., Wang, R., and Zhou, J.: Evapotranspiration Measurement and Crop Coefficient Estimation over a Spring  
648 Wheat Farmland Ecosystem in the Loess Plateau, *PLoS ONE*, 9, e100031, <https://doi.org/10.1371/journal.pone.0100031>,  
649 2014.

650 Yasuda, T., Yonemura, S., and Tani, A.: Comparison of the Characteristics of Small Commercial NDIR CO<sub>2</sub> Sensor Models  
651 and Development of a Portable CO<sub>2</sub> Measurement Device, *Sensors*, 12, 3641–3655, <https://doi.org/10.3390/s120303641>,  
652 2012.